Article:
Abdalla, I, Corda, J and Zhang, L (2016) Optimal control of a multilevel DC-link converter photovoltaic system for maximum power generation. Renewable Energy, 92. pp. 1-11. ISSN 0960-1481

https://doi.org/10.1016/j.renene.2016.01.062

Optimal Control of a Multilevel DC-Link Converter Photovoltaic System for Maximum Power Generation

I Abdalla, J Corda, L Zhang

School of Electronic and Electrical Engineering, University of Leeds
Leeds LS2 9JT, United Kingdom
E-mail: l.zhang@leeds.ac.uk

Abstract

This paper describes a new algorithm for optimal control of a PV system under partial shading. A multilevel DC-link is the essential part of the proposed system and its control engages a voltage-hold perturbation and observation (VH-P&O) method combined with a PWM algorithm with permutation of PV sources. The algorithm enables achieving the maximum power generation for any number of PV and converter modules. The main features of the control are: (i) a continual operation of all PV sources, shaded and non-shaded, at their maximum power points, (ii) delivery of all extracted power from PV sources to the load and (iii) generation of multilevel output voltage waveform with a low total harmonic distortion.

Keywords: Multilevel Converters, MPPT, Partial Shading, Photovoltaic Panels

1 Introduction

PV power generators are commonly structured by connecting the PV modules in series to meet the load voltage requirement. This configuration constrains that the same current flows through the chain. However, the characteristics of the chained PV modules are not exactly identical even when they are manufactured in the same batch. A more profound issue is the levels of illumination on individual PV cells which may be different. Even if a single cell in the series chain is shaded, the current through the whole chain would be reduced according to the shaded cell and consequently the overall power output of the whole PV chain drops significantly. Furthermore the shaded cell or cells may be destroyed due to the increased power dissipation on them resulting hot spots. A classical method to prevent high power dissipation on shaded cells has been to connect bypass diodes across a set of chained cells

(normally 18). The drawback of such a method is that under uneven irradiance, when diode/s turn on to allow the current flowing through, the power from individual cells is lost.

Various other methods have been developed to address the problem of partial shading. One of them uses the Module-Integrated PV Converter (MIPC) scheme [1 - 4] which is formed from a series connection of modules comprising a PV panel and a DC/DC converter. This enables the control of each PV source output voltage for maximum power generation, while maintaining the same current value at the converter output terminal. However the problem with this scheme is that the converter for the shaded PV panel may only be able to maintain the current equal to that of the other modules when the irradiance difference is moderate.

Departure from the maximum power point (MPP) may be unavoidable for a shaded source with a larger light level discrepancy, and in this case the option may be to control the converter to bypass the shaded source. Another approach relies on connecting the PV sources into a number of clusters of nearly equal extracted power by using a switching matrix to reconfigure the clusters so that the PV sources of equal shading, hence equal power generation, are connected in parallel. The method was presented in [5, 6] and implemented experimentally in [7]. Although tests have shown that this approach results in more power output than in the directly connected PV sources, the cluster which generates the least power will be bypassed completely. The third scheme, named the 'Generation Control Circuit' (GCC), uses a type of multilevel DC/DC converter with multiple DC/DC converters connected in series, each powered by a PV source [8]. The individual converter may be a buck-boost type and can be controlled to extract power from the PV sources and deliver it to the load directly. This idea was implemented in [9] using a fly-back converter allocated to each PV source. The main issue with this scheme is that the PV sources cannot be controlled completely independently. Consequently, locating the MPP of one PV source does not mean that the other PV sources operate at their MPPs.

This paper presents a novel optimal control scheme for a PV system using a converter topology called the multilevel DC-link inverter. Similar to the MIPC above this system consists of multiple modules

connected in series, each module has a PV panel with a switch-diode pair at its output terminals. A DC-AC bridge inverter is used at the output to convert the generated DC power into AC form [10]. The topology and control strategy enables the system to achieve the MPP tracking for all PV sources in a system under any irradiation conditions. An initial investigation [11] has demonstrated the basic converter topology and control concept. It has been shown that the scheme allows flexible control of each PV source to make it operating at its respective MPP corresponding to its light level. In the current paper a further improved control algorithm is presented which combines a voltage-hold perturbation and observation (VH-P&O) method and the PWM algorithm with permutation of PV sources for achieving the maximum power generation for any number of converter levels. The method is presented by both simulation study and practical experimental test, and the results show a significant enhancement of the PV system performance.

The paper is organised as follows. Section 2 describes the multilevel DC-link inverter topology. In Section 3 the new control algorithm which combines the VH-P&O scheme and permutation PWM strategy is presented in detail. Simulation study of the PV system and the control scheme, which is performed using a STATE-SPACE AVERAGE model for the multilevel DC-link inverter, together with the results obtained are discussed in Section 4. Finally, the experimental system and results obtained by testing are presented in Section 5.

2 Structure of the PV System based on Multilevel DC-Link Converter

Fig. 1 shows the configuration of a PV system comprising three PV units acting in conjunction with a multilevel DC-link converter. Each PV unit consists of a single PV source, a capacitor and a switch with a complimentary diode. The units are connected in series and any of them can be switched in or out of the chain by turning on or off its switch. When a unit is switched off, it is being bypassed by a diode. The three switches (SW1, SW2, SW3) operate at a high frequency and are controlled by the direct PWM method [12] to form a three-level positive DC voltage. The H–bridge inverter at the output serves to convert the multilevel DC voltage waveform to alternative positive and negative

output voltage half-cycles of the required output frequency (e.g. 50Hz). The generation of multiple voltage levels, combined with proper control, enables forming the approximate sinewave output.

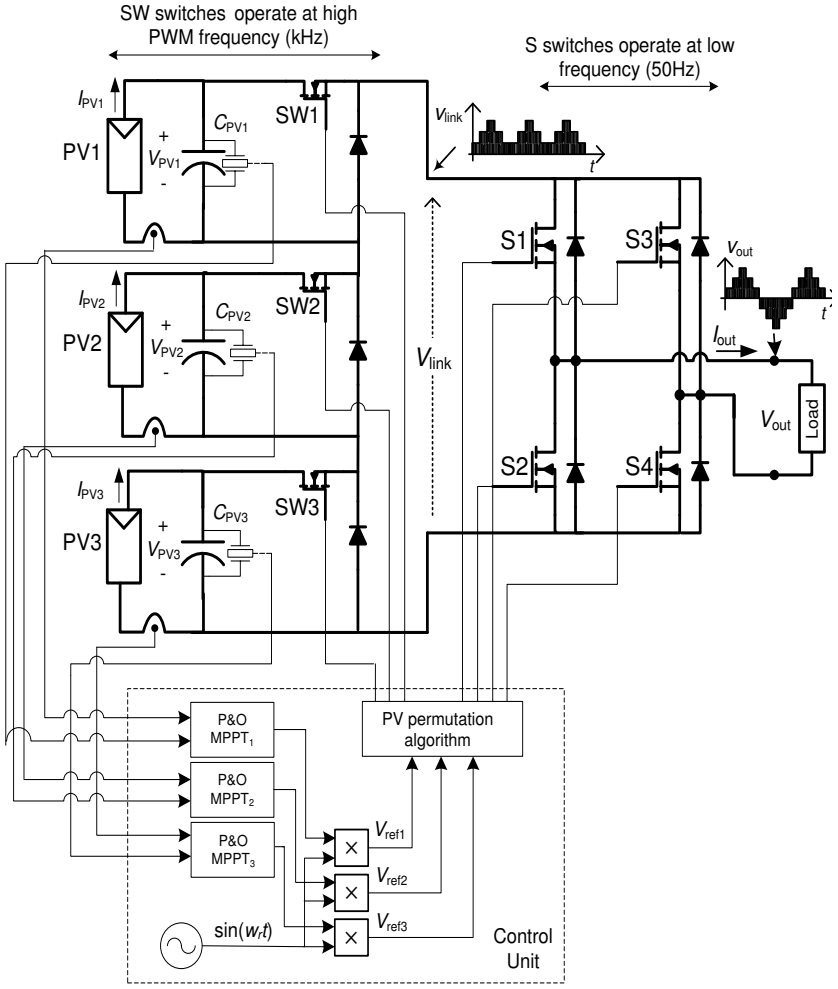

Fig. 1: PV system with multilevel DC- link converter

3 Optimal Control Scheme based on Permutation of PV Sources

The optimal control scheme should maximise the power transferred from PV sources to the AC load or grid in different light conditions, and generate a nearly sinusoidal voltage with minimum harmonic distortion and DC offset. Ideally, it should also ensure equal switching utilisation and hence the losses. The solution presented in this paper comprises two parts: (i) Voltage-Hold Perturb & Observe (VH P&O) method for generation of the MPP reference voltage and (ii) PWM algorithm with permutation of PV sources for switching control.

3.1 The Voltage-Hold P&O Method for Reference Voltage Generation

A classical strategy for the PV maximum power point tracking is the perturbation and observation (P&O) method, which has been widely studied and used in the PV MPPT controllers (e.g. [13-17]). The two problems linked with this simple search method are that the terminal voltage may oscillate around a MPP, and the system may lose the MPP during rapid irradiance changes. Some improvements have been proposed for reducing the number of oscillations around MPP (e.g. [18, 19]), but a slow speed of the response may result in an incorrect MPPT if the changes of irradiance are rapid.

The voltage-hold (VH) P&O method proposed here overcomes the above limitation in terms of oscillations around MPPs, which cause noise and slow down the search process, and also it can cope with rapid irradiance changes. For solving the problem of oscillating around a MPP, the algorithm uses variable searching step size. As soon as the irradiation change stops, the tracking step size is gradually decreased towards zero when reaching close to the MPP. When an irradiation change occurs, the tracking step size will be reset to the initial value to maintain the fast tracking. At a rapid irradiance change, which can be detected by measuring the light level and the number of changes within a fixed time interval, the algorithm stops the searching process and sets the reference voltage to the measured PV capacitor voltage which is essential tracking quantity. Subsequently the algorithm resumes the perturbation process for searching the MPP voltage along the I-V characteristic corresponding to the new light level.

The VH P&O method is applied in sequence to each PV unit at each sampling instant, to track individually their respective reference voltages. This may lead to different voltage values depending on the weather conditions and PV panel characteristics. For generating AC reference voltages these values are multiplied by a unity sinusoidal signal $\sin \omega t$ ($\omega = 2\pi \times 50$). (For example, in the system with three PV units, the reference voltages $v_{ref1}(t)$, $v_{ref2}(t)$ and $v_{ref3}(t)$ are generated as shown in Fig.1.)

3.2 PWM Algorithm with Permutation of PV Sources

The next step should naturally be generation of PWM signals for the switches of individual PV units. For maximum power extraction, the terminal voltage of each PV unit should be as close as possible to its individual reference voltage established by the VH P&O process. This also implies that with multiple PV units in a chain, the PWM reference signal for the whole system should be the sum of all individual reference voltages, i.e. $v_{ref1}(t)+ v_{ref2}(t),\ldots+ v_{ref(n)}(t)$. To meet these conditions and the criteria of equal switch utilisation and low waveform distortion, a novel PWM algorithm based on permutation of PV sources has been developed. The algorithm consists of three stages, which are performed within each PWM switching period T_s: the direct PWM [12], the sequential permutation of PV sources, and the AC output voltage generation.

In Stage 1, the direct PWM determines the output voltage levels and switch-on time intervals as follows. The reference voltages $v_{ref(j)}(t)$ (j = 1,…n), obtained from VH P&O process, are normalised as

$$\bar{v}_{ref(j)} = \frac{\left|v_{ref(j)}(t)\right|}{V_L / n} \qquad (1)$$

where the standard voltage level V_L equals V_{MPP} for a single source (panel) at the standard irradiance of 1000 W/m^2 and temperature 25ºC, and n is the total number of PV sources. (This makes normalised voltages $n\times v_{ref(j)}/V_L$, i.e. they are normalized for the full system comprising n sources.)

The integer part of each normalized reference voltage is defined as the offset voltage, i.e.

$$v_{offset(j)} = \mathrm{int}[\bar{v}_{ref(j)}] \qquad (2)$$

If $v_{offset(j)} > 1$, the switch of the corresponding PV source should be in 'on' state during time interval

$$t_{on(j)} = T_s \times (\bar{v}_{ref(j)} - v_{offset(j)}) \qquad (3)$$

On the other hand if $v_{offset(j)} = 0$, the switch of the corresponding PV source should be in 'off' state to allow the diode to bypass this source. Stage 1 generates all n values of $v_{offset(j)}$ and $t_{on(j)}$.

In Stage 2, the sequential permutation algorithm is implemented to determine the switching states of all PV units for building up the output voltage of the system. All PV sources are sequentially permutated through consecutive PWM switching cycles according to the cyclic counter C as

illustrated in Fig.2. The PV source which sequentially comes in turn at the highest voltage level is the only one which is controlled at a particular switching period (T_s), while other sources are used to build up the appropriate voltage level. The benefits of such a process are: (i) all PV sources of the system are equally engaged and the switching losses of transistors associated with each PV source are balanced, (ii) the achievement of symmetrical positive and negative half-cycles of the AC output waveform under partial shading and (iii) the reduction of the voltage ripple on capacitors of PV units.

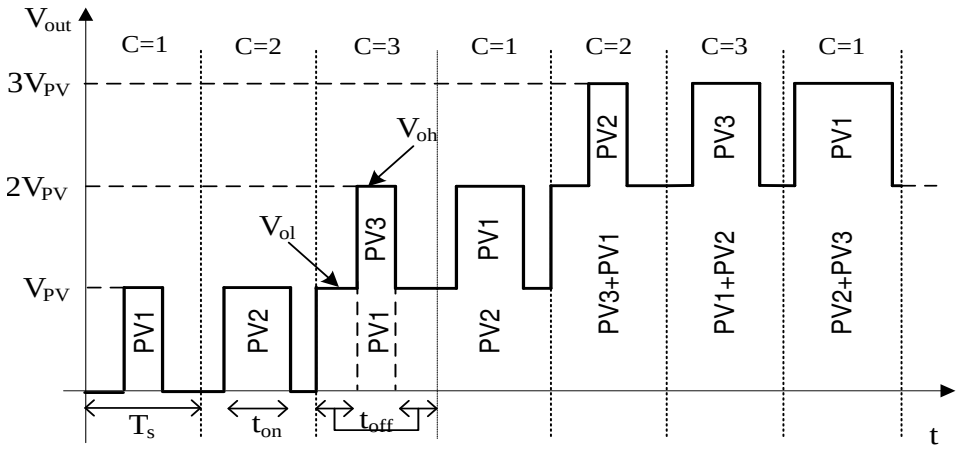

Fig. 2: Permutation of PV sources through consecutive PWM switching cycles

Unlike the basic algorithm [11], the improved algorithm does not represent the PV source at the output if its offset voltage is zero, except in the case when all offset voltages are zero. The reason for introducing this exception is to initiate the control and it is also required in the case of low PWM reference signals.

In Stage 3 the terminal H-bridge converter is used to change the multilevel DC voltage waveform to a single-phase AC waveform of low frequency (e.g. 50 Hz) by tracking the sinusoidal reference signal.

Table 1 presents the switching states and output voltage generation for the system with three PV sources ($n = 3$). According to formulae (1) - (2), the offset voltages $v_{offset(j)}$ ($j = 1,2,3$) can be either 0, 1 or 2. Hence there are 27 combinations in total and 27 output voltage patterns, which makes the presentation quite cumbersome. For clarification, a graphical illustration of the process for generating the output waveform in the basic system with two PV sources is given in the Appendix.

C	$v_{offset1}$	$v_{offset2}$	$v_{offset3}$	V_{ol}	V_{oh}	t_{on}
1	0	0	0	0	V_{PV1}	t_{on1}
	0	0	1	0	0	
	0	0	2	V_{PV3}	V_{PV3}	
	0	1	0	V_{PV2}	V_{PV2}	
	0	1	1	V_{PV2}	V_{PV2}	
	0	1	2	V_{PV2}+V_{PV3}	V_{PV2}+V_{PV3}	
	0	2	0	V_{PV2}	V_{PV2}	
	0	2	1	V_{PV2}+V_{PV3}	V_{PV2}+V_{PV3}	
	0	2	2	V_{PV2}+V_{PV3}	V_{PV2}+V_{PV3}	
	1	0	0	0	V_{PV1}	
	1	0	1	0	V_{PV1}	
	1	0	2	V_{PV3}	V_{PV1}+ V_{PV3}	
	1	1	0	V_{PV2}	V_{PV1}+ V_{PV2}	
	1	1	1	V_{PV2}	V_{PV1}+ V_{PV2}	
	1	1	2	V_{PV2}+V_{PV3}	V_{PV1}+ V_{PV2}+ V_{PV3}	
	1	2	0	V_{PV2}	V_{PV1}+ V_{PV2}	
	1	2	1	V_{PV2}+V_{PV3}	V_{PV1}+ V_{PV2}+ V_{PV3}	
	1	2	2	V_{PV2}+V_{PV3}	V_{PV1}+ V_{PV2}+ V_{PV3}	
	2	0	0	0	V_{PV1}	
	2	0	1	V_{PV3}	V_{PV1}+ V_{PV3}	
	2	0	2	V_{PV3}	V_{PV1}+ V_{PV3}	
	2	1	0	V_{PV2}	V_{PV1}+ V_{PV2}	
	2	1	1	V_{PV2}+V_{PV3}	V_{PV1}+ V_{PV2}+ V_{PV3}	
	2	1	2	V_{PV2}+V_{PV3}	V_{PV1}+ V_{PV2}+ V_{PV3}	
	2	2	0	V_{PV2}	V_{PV1}+ V_{PV2}	
	2	2	1	V_{PV2}+V_{PV3}	V_{PV1}+ V_{PV2}+ V_{PV3}	
	2	2	2	V_{PV2}+V_{PV3}	V_{PV1}+ V_{PV2}+ V_{PV3}	
2	0	0	0	0	V_{PV2}	t_{on2}
	0	0	1	V_{PV3}	V_{PV3}	
	0	0	2	V$_{PV3}$	V_{PV3}	
	0	1	0	0	V_{PV2}	
	0	1	1	V_{PV3}	V_{PV2}+V_{PV3}	
	0	1	2	V_{PV3}	V_{PV2}+V_{PV3}	
	0	2	0	0	V_{PV2}	
	0	2	1	V_{PV3}	V_{PV2}+V_{PV3}	
	0	2	2	V_{PV3}	V_{PV2}+V_{PV3}	
	1	0	0	0	0	
	1	0	1	V_{PV3}	V_{PV3}	
	1	0	2	V_{PV1}+V_{PV3}	V_{PV1}+V_{PV3}	
	1	1	0	0	V_{PV2}	
	1	1	1	V_{PV3}	V_{PV2}+ V_{PV3}	
	1	1	2	V_{PV1}+V_{PV3}	V_{PV1}+ V_{PV2}+ V_{PV3}	
	1	2	0	V_{PV1}	V_{PV1}+ V_{PV2}	
	1	2	1	V_{PV1}+V_{PV3}	V_{PV1}+ V_{PV2}+ V_{PV3}	
	1	2	2	V_{PV1}+V_{PV3}	V_{PV1}+ V_{PV2}+ V_{PV3}	
	2	0	0	V_{PV1}	V_{PV1}	
	2	0	1	V_{PV1}+V_{PV3}	V_{PV1}+ V_{PV3}	
	2	0	2	V_{PV1}+V_{PV3}	V_{PV1}+ V_{PV3}	
	2	1	0	V_{PV1}	V_{PV1}+ V_{PV2}	
	2	1	1	V_{PV1}+V_{PV3}	V_{PV1}+ V_{PV2}+ V_{PV3}	
	2	1	2	V_{PV1}+V_{PV3}	V_{PV1}+ V_{PV2}+ V_{PV3}	
	2	2	0	V_{PV1}	V_{PV1}+V_{PV2}	
	2	2	1	V_{PV1}+V_{PV3}	V_{PV1}+ V_{PV2}+ V_{PV3}	
	2	2	2	V_{PV1}+V_{PV3}	V_{PV1}+ V_{PV2}+ V_{PV3}	

Continued …

C	$v_{offset1}$	$v_{offset2}$	$v_{offset3}$	V_{ol}	V_{oh}	t_{on}
3	0	0	0	0	V_{PV3}	t_{on3}
	0	0	1	0	V_{PV3}	
	0	0	2	0	V_{PV3}	
	0	1	0	0	0	
	0	1	1	0	V_{PV3}	
	0	1	2	V_{PV2}	V_{PV2}+V_{PV3}	
	0	2	0	V_{PV2}	V_{PV2}	
	0	2	1	V_{PV2}	V_{PV2}+V_{PV3}	
	0	2	2	V_{PV2}	V_{PV2}+V_{PV3}	
	1	0	0	V_{PV1}	V_{PV1}	
	1	0	1	V_{PV1}	V_{PV1}+ V_{PV3}	
	1	0	2	V_{PV1}	V_{PV1}+ V_{PV3}	
	1	1	0	V_{PV1}	V_{PV1}	
	1	1	1	V_{PV1}	V_{PV1}+ V_{PV3}	
	1	1	2	V_{PV1}+V_{PV2}	V_{PV1}+ V_{PV2}+ V_{PV3}	
	1	2	0	V_{PV1}+V_{PV2}	V_{PV1}+ V_{PV2}	
	1	2	1	V_{PV1}+V_{PV2}	V_{PV1}+ V_{PV2}+ V_{PV3}	
	1	2	2	V_{PV1}+V_{PV2}	V_{PV1}+ V_{PV2}+ V_{PV3}	
	2	0	0	V_{PV1}	V_{PV1}	
	2	0	1	V_{PV1}	V_{PV1}+ V_{PV3}	
	2	0	2	V_{PV1}	V_{PV1}+ V_{PV3}	
	2	1	0	V_{PV1}+V_{PV2}	V_{PV1}+ V_{PV2}	
	2	1	1	V_{PV1}+V_{PV2}	V_{PV1}+ V_{PV2}+ V_{PV3}	
	2	1	2	V_{PV1}+V_{PV2}	V_{PV1}+ V_{PV2}+ V_{PV3}	
	2	2	0	V_{PV1}+V_{PV2}	V_{PV1}+ V_{PV2}	
	2	2	1	V_{PV1}+V_{PV2}	V_{PV1}+ V_{PV2}+ V_{PV3}	
	2	2	2	V_{PV1}+V_{PV2}	V_{PV1}+ V_{PV2}+ V_{PV3}	

Table 1: Switching states and output voltage generation for the system with three PV sources

4 Simulation of the PV System Performance

The multilevel DC-link converter is simulated using a state-space average (SSA) model having the general form given by [20]:

$$\begin{bmatrix} \frac{dv_{pv1}}{dt} \\ \frac{dv_{pv2}}{dt} \\ \cdot \\ \cdot \\ \cdot \\ \frac{dv_{pv(n)}}{dt} \end{bmatrix} = \frac{1}{R} \begin{bmatrix} \frac{-D_1^2}{C_{pv1}} & \frac{-D_1D_2}{C_{pv1}} & \cdots & \frac{-D_1D_n}{C_{pv1}} \\ \frac{-D_2D_1}{C_{pv2}} & \frac{-D_2^2}{C_{pv2}} & \cdots & \frac{-D_2D_n}{C_{pv2}} \\ \cdot & \cdot & \cdots & \cdot \\ \cdot & \cdot & \cdots & \cdot \\ \cdot & \cdot & \cdots & \cdot \\ \frac{-D_nD_1}{C_{pv(n)}} & \frac{-D_nD_2}{C_{pv(n)}} & \cdots & \frac{-D_n^2}{C_{pv(n)}} \end{bmatrix} \begin{bmatrix} v_{pv1} \\ v_{pv2} \\ \cdot \\ \cdot \\ \cdot \\ v_{pv(n)} \end{bmatrix} + \begin{bmatrix} \frac{1}{C_{pv1}} & 0 & \cdots & 0 \\ 0 & \frac{1}{C_{pv2}} & \cdots & 0 \\ 0 & 0 & \cdots & \cdot \\ 0 & 0 & \cdots & \cdot \\ 0 & 0 & \cdots & 0 \\ 0 & 0 & 0 & \frac{1}{C_{pv(n)}} \end{bmatrix} \begin{bmatrix} i_{pv1} \\ i_{pv2} \\ \cdot \\ \cdot \\ \cdot \\ i_{pv(n)} \end{bmatrix} \quad (4)$$

$$[v_{out}] = (2D-1)[D_1 \;\; D_2 \;\; \cdots \;\; D_n] \begin{bmatrix} v_{pv1} \\ v_{pv2} \\ \vdots \\ v_{pv(n)} \end{bmatrix} \quad (5)$$

where, the input vector elements are the currents i_{pv1}, i_{pv2},…$i_{pv(n)}$ of PV sources; the terminal voltages v_{pv1}, v_{pv2},…$v_{pv(n)}$ form the state vector; C_{pv1}, C_{pv2},…$C_{pv(n)}$ are the corresponding terminal capacitances; D_l, D_2, ... D_n are the state variables for switches SW_1, SW_2… $SW_{(n)}$; R is the load resistance; D is the state variable of the single-phase output H-bridge inverter (D = 1 when S1&S4 are switched on, and D = 0 when S2&S3 are switched on).

Elements of the input vector [i_{pv1}, i_{pv2},…$i_{pv(n)}$] are found from the MPPs of the I-V characteristics which are generated using Bishop's model for the PV source [21]. The I-V characteristics for different irradiance levels are shown in Fig.3 with indicated MPPs. Table 2 lists the system parameters used in the model.

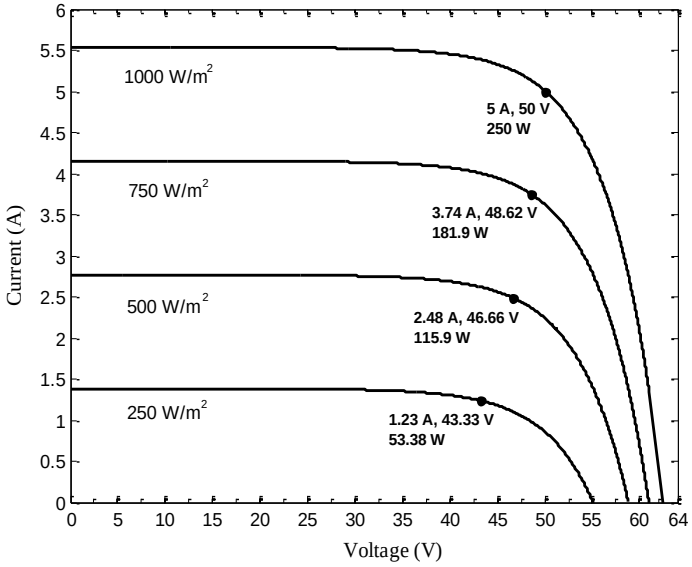

Fig. 3: I-V characteristics of the PV source for different irradiance levels (MPP is indicated on each characteristic.)

Symbol	Parameter	Value
P_{MPP}	Maximum power of PV source	250 W
C_{pv}	PV source terminal capacitor	5500 μF
R	Load resistance	8.5 Ω (5&7-level) 18.5 Ω (9-level) 23 Ω (11-level)
e_v	P&O tracking step size	0.5 V
M_f	Frequency modulation index	100 (5-level) 300 (7,9&11-level)
f	AC output frequency	50 Hz

Table 2: PV system parameters used in simulations

The waveforms were simulated for the PV systems with n = 2, 3, 4 and 5 sources generating respectively five, seven, nine and eleven-level AC output voltages. The Fast Fourier Transformation (FFT) is applied to the output waveform to evaluate the fundamental harmonic and the total harmonics distortion (THD).

Fig. 4a shows five-level output voltage waveforms produced by the system with two sources PV1 and PV2 exposed to irradiances of 500 W/m^2 and 1000 W/m^2 respectively. The improved algorithm gives better voltage waveforms (shown on the right) compared with its predecessor. The THD of 43.5% and the 50-Hz fundamental peak voltage $V_{1(p)}$ = 76.8 V were achieved with the improved algorithm, compared to the THD of 58.65% and $V_{1(p)}$ = 70.7 V achieved with the predecessor. Similar comparison was made for the seven-level converter with three PV sources at irradiances of 1000, 500 and 1000 W/m^2 applied to PV1, PV2 and PV3 respectively. The output voltage waveforms are shown in Fig. 4b. The improved algorithm generates substantially better waveform with THD = 35.72% and $V_{1(p)}$ = 108.64 V, compared to the THD = 57.41% and $V_{1(p)}$ = 95.81 V achieved with the predecessor.

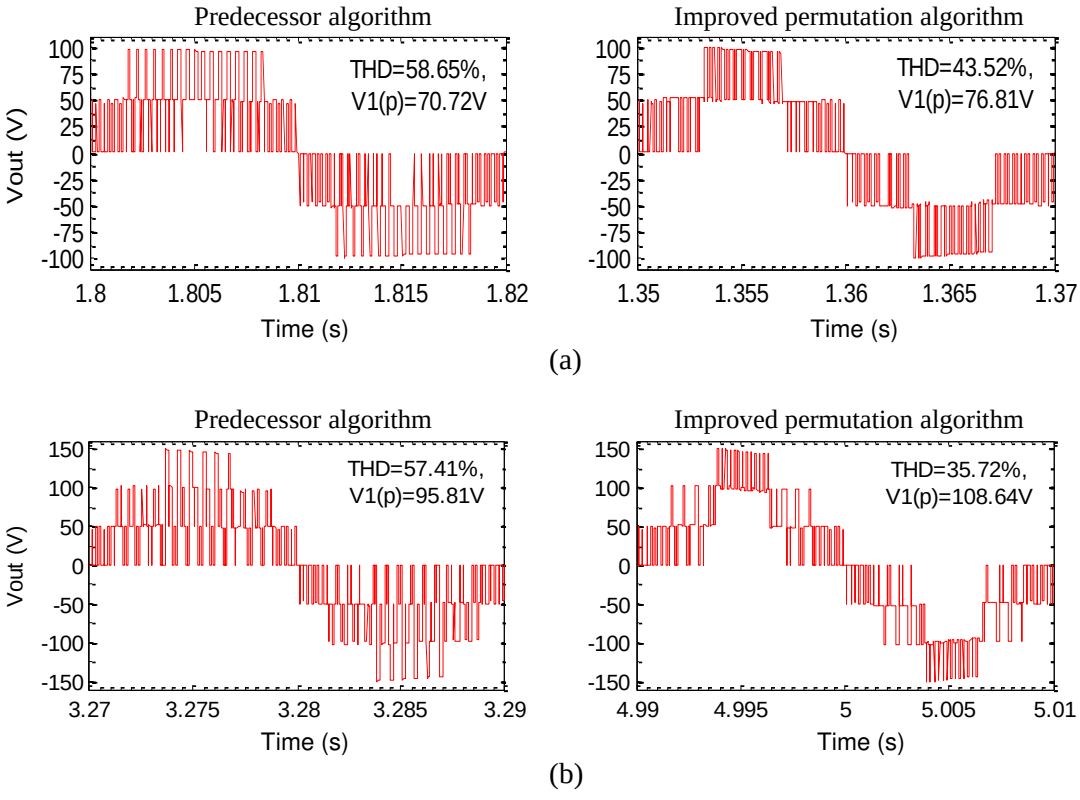

Fig. 4: Output voltage waveforms simulated by the predecessor and the improved algorithm.

(a) five-level AC waveforms with sources PV1 and PV2 at irradiances 500 and 1000 W/m^2;

(b) seven-level AC waveforms with sources PV1, PV2 and PV3 at irradiances 1000, 500 and 1000 W/m^2 respectively.

Fig. 5 illustrates output voltage waveforms and power extracted from the system with four PV sources using 9-level converter for two cases – (a) none of the sources are shaded and (b) one source is shaded. The power levels extracted from individual sources and the load power are shown by line graphs on the right-hand side. Referring to Fig. 5a, when all four PV sources are exposed to equal irradiance of 1000 W/m2, the THD is 18.4%, the 50-Hz fundamental peak voltage V1(p) = 194 V and the power extracted from each panel is 250 W giving 1000 W to the load. Referring to Fig. 5b, when one source is shaded, i.e. exposed to the halved irradiance (500 W/m2), the predicted THD is 21.67%, V1(p) = 176 V and the total power delivered to the load is 865 W conforming that it is very close to the sum of maximum power values found from I-V characteristics (3x250+116 W).

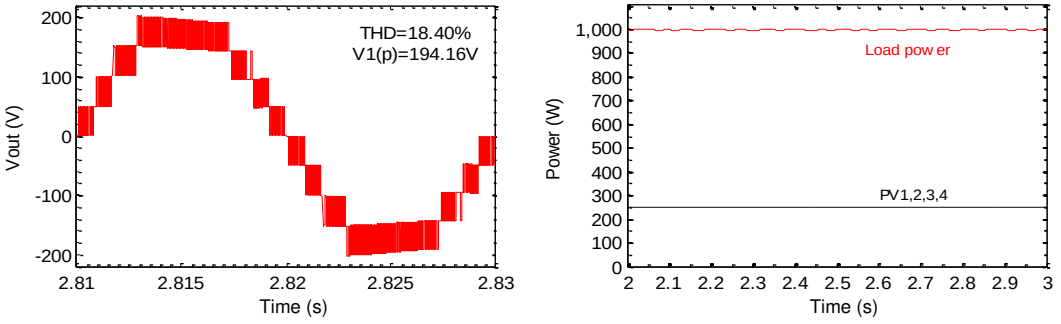

(a)

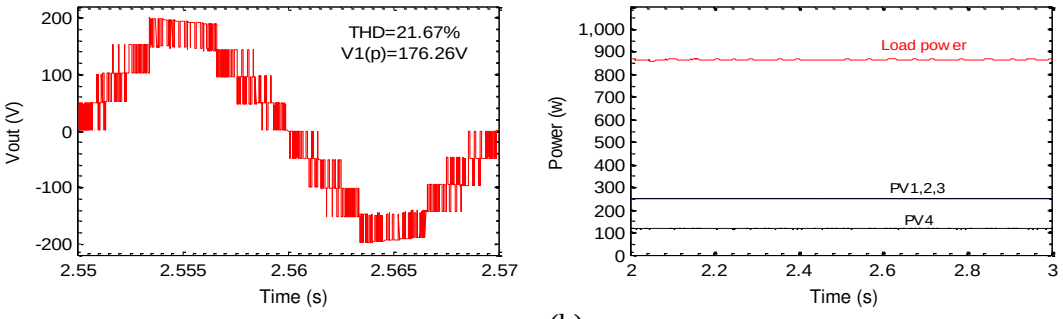

(b)

Fig. 5: Simulated output voltage waveforms and the extracted power achieved by the improved algorithm for 9-level converter with four PV sources.

(a) all at the same irradiance of 1000W/m^2;

(b) at irradiances of 1000 W/m^2 for PV1, PV2, PV3 and 500W/m^2 for PV4.

Fig. 6 illustrates another example, which relates to the system with five PV sources and using 11-level converter. Referring to Fig. 6a, when all sources are exposed to equal irradiance of 1000 W/m^2, the values of THD and the 50-Hz fundamental peak voltage $V_{1(p)}$ are respectively 14.95% and 241 V and both are improved compared to the values achieved by 9-level converter (18.4% and 194 V). Fig. 6b relates to the state when PV sources are exposed to different irradiances (250, 500, 750, 750 and 1000 W/m^2). The predicted THD is now 19.48%, and the total power delivered to the load is 790W which is very close to the sum of maximum power values of five PV sources found from I-V characteristics (53W, 116 W, 2x182 W and 250 W).

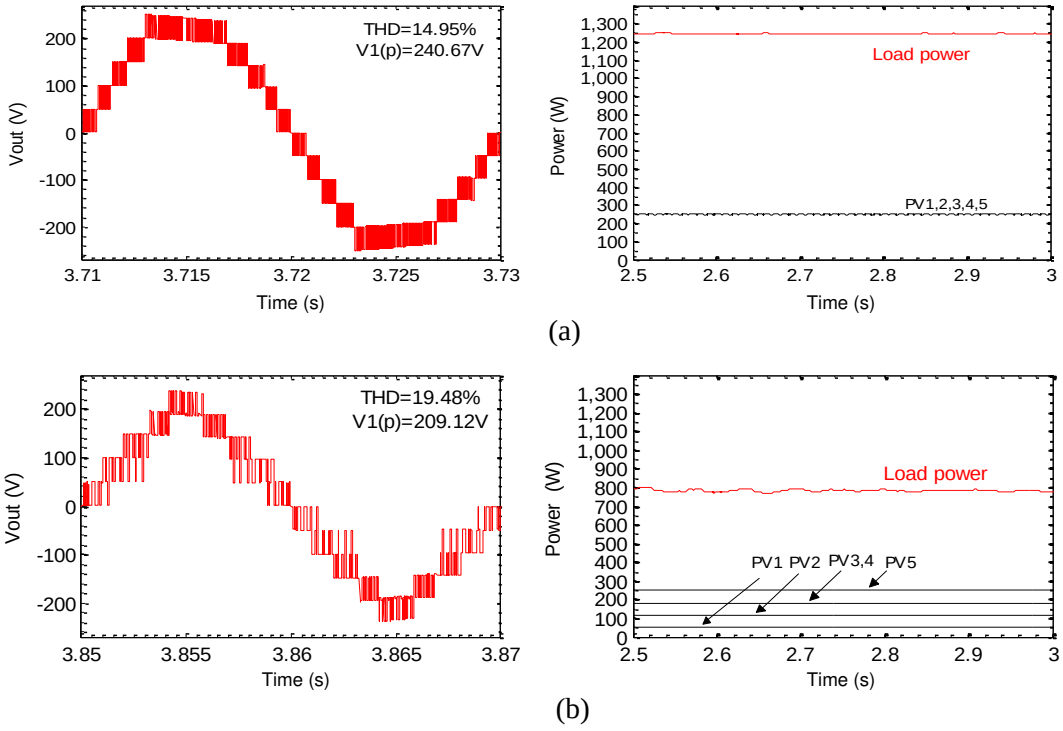

Fig. 6: Simulated output voltage waveforms and the extracted power achieved by the improved algorithm for 11-level converter with five PV sources.

(a) all at the same irradiance of 1000W/m^2;

(b) at irradiances of 250, 500, 750, 750 and 1000 W/m^2.

Fig. 7 illustrates the dynamic performance in terms of extracted power from each PV source and the total power delivered to the load from 7-level converter for a sequence of irradiance variations. Initially the full irradiance of 1000 W/m2 is applied to all three PV sources and 250 W is extracted

from each source delivering a total of 750 W to the load. In the time between 2 and 5 seconds, the irradiance to PV3 source is halved (500 W/m2), while PV1 and PV2 are still at full irradiance. The extracted power from PV3 is now reduced to 116 W, which matches the MPP on the I-V characteristic at irradiance of 500 W/m2 in Fig.3. The power levels from PV1 and PV2 are not affected by the shading of PV3, so the total delivered power is 616 W. During the time interval between 5 and 8 seconds, both PV2 and PV3 are shaded at the halved irradiance (500 W/m2) while PV1 is under full irradiance, and the delivered power is 482 W. Between 8 and 11 seconds, all three PV sources are shaded to the halved irradiance (500W/m2), and the power delivered to the load is reduced to 348 W. After 11 seconds all three PV sources are again exposed to the full irradiance and are recovered to their MPPs of 250 W delivering the power of 750 W to the load.

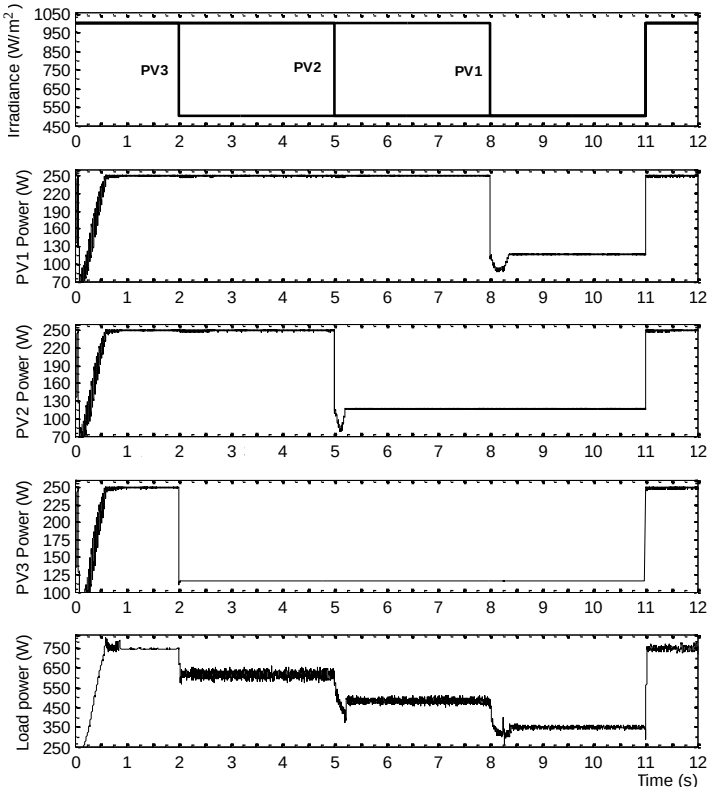

Fig. 7. Power responses of the system with seven-level DC-link converter during irradiance changes.

(a) irradiance variations in time;

(b)-(d) extracted power from individual sources PV1, PV2 and PV3;

(e) total power delivered to the load.

5 Experimental Results

Laboratory experiments were performed on a system having three identical small serially connected PV modules (sources) with an in-house built 7-level converter. Each module was exposed to a separate artificial sunlight with adjustable irradiance emulated by three halogen bulbs each of which was supplied from a different phase of a 3-phase variac connected to the 3-phase 50-Hz mains supply. This arrangement provides a fairly uniform irradiance to each module.

The parameters of the experimental system are listed in Table 3. The measured I-V characteristic of the PV module are shown in Fig. 8 under different irradiance levels at room and surface temperatures of 20°C and 38°C respectively.

Symbol	Quantity	Value
P_{MPP}	PV source maximum power	10 W
C_{pv}	PV source terminal capacitor	2200 μF
R	Load resistance	30 Ω
e_v	P&O tracking step size	0.2 V
M_f	Frequency modulation index	100
f	Output frequency	50 Hz

Table 3: Experimental system parameters

Though the power ratings of the PV panels are lower than those used in the simulation study, this is considered adequate for verifying the principle of the proposed control scheme for the following reasons: (i) With the artificial sun light simulator set up in the available laboratory, the measured I-V characteristics of small PV panels corresponding to various light and temperature levels follow closely the characteristics given in the data sheets. However, panels with higher power rating (over 100 W) give significantly lower output power compared to what they should generate based on the data sheet; (ii) For validating the proposed control scheme the difference in power rating is not considered an issue, because the controller can be scaled up for higher power system without causing dynamic stability problems.

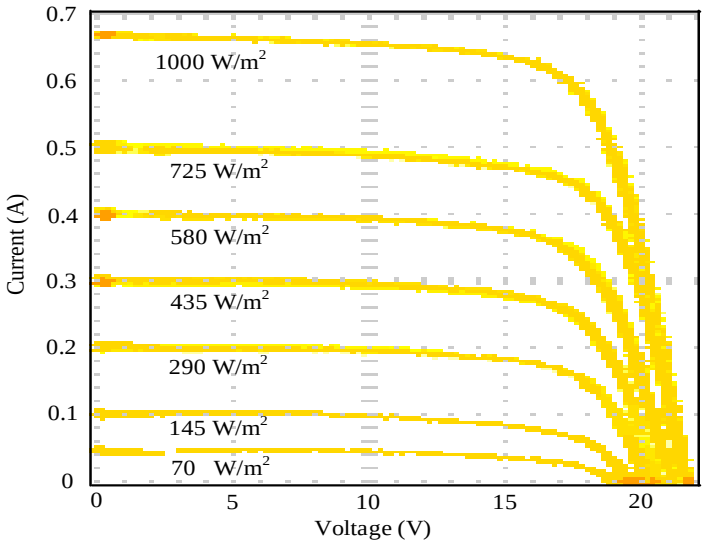

Fig. 8. Measured I-V characteristic of a 10W PV module at different irradiances

The improved control algorithm has been applied to the experimental system. The control is implemented via a digital processing unit eZdsp^{TM} F28335 in real-time [22], and the Matlab-Simulink real time data exchange (RTDX) is employed to display the extracted power and to modify the system parameters via a graphical user interface (GUI). Details of this are presented in [21].

The extracted power from each PV module can be monitored on the bar chart of the GUI window in real-time mode as illustrated in Fig. 9 which shows two examples with different shading conditions. The graphs demonstrate that the developed system ensures that shaded PV module/s do not affect the operation of non-shaded module/s which continue to generate their maximum power.

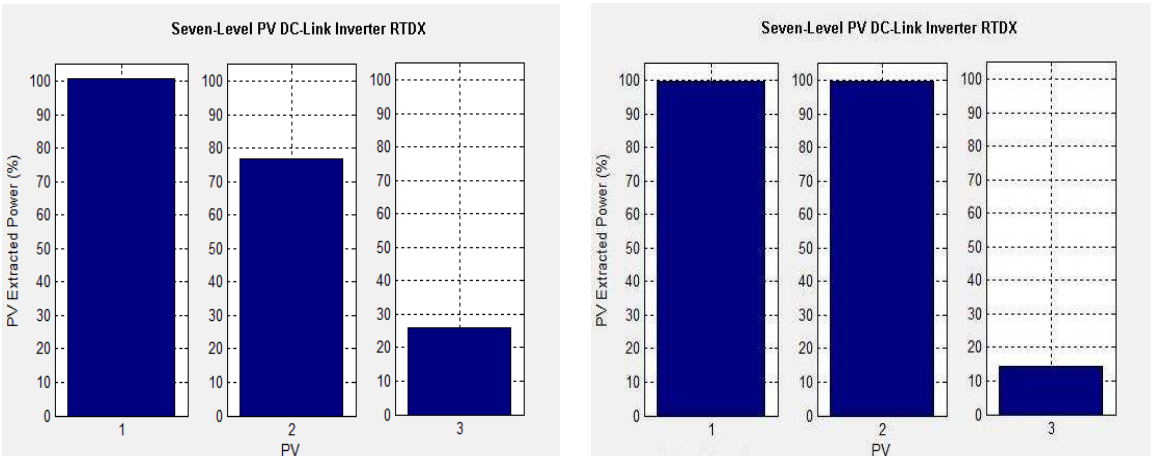

Fig. 9: GUI window showing the extracted power from each PV module at different irradiances

Table 4 summarizes the THD and the 50Hz fundamental amplitude of the load voltage waveforms which are shown in Fig. 10 for both the previous and improved PV permutation algorithms as a function of the PV extracted power. It is apparent that at the same conditions of partial shading, the improved PV permutation algorithm has resulted in a lower output harmonic distortion and larger amplitude of the fundamental harmonic (50 Hz), compared to the precursor algorithm.

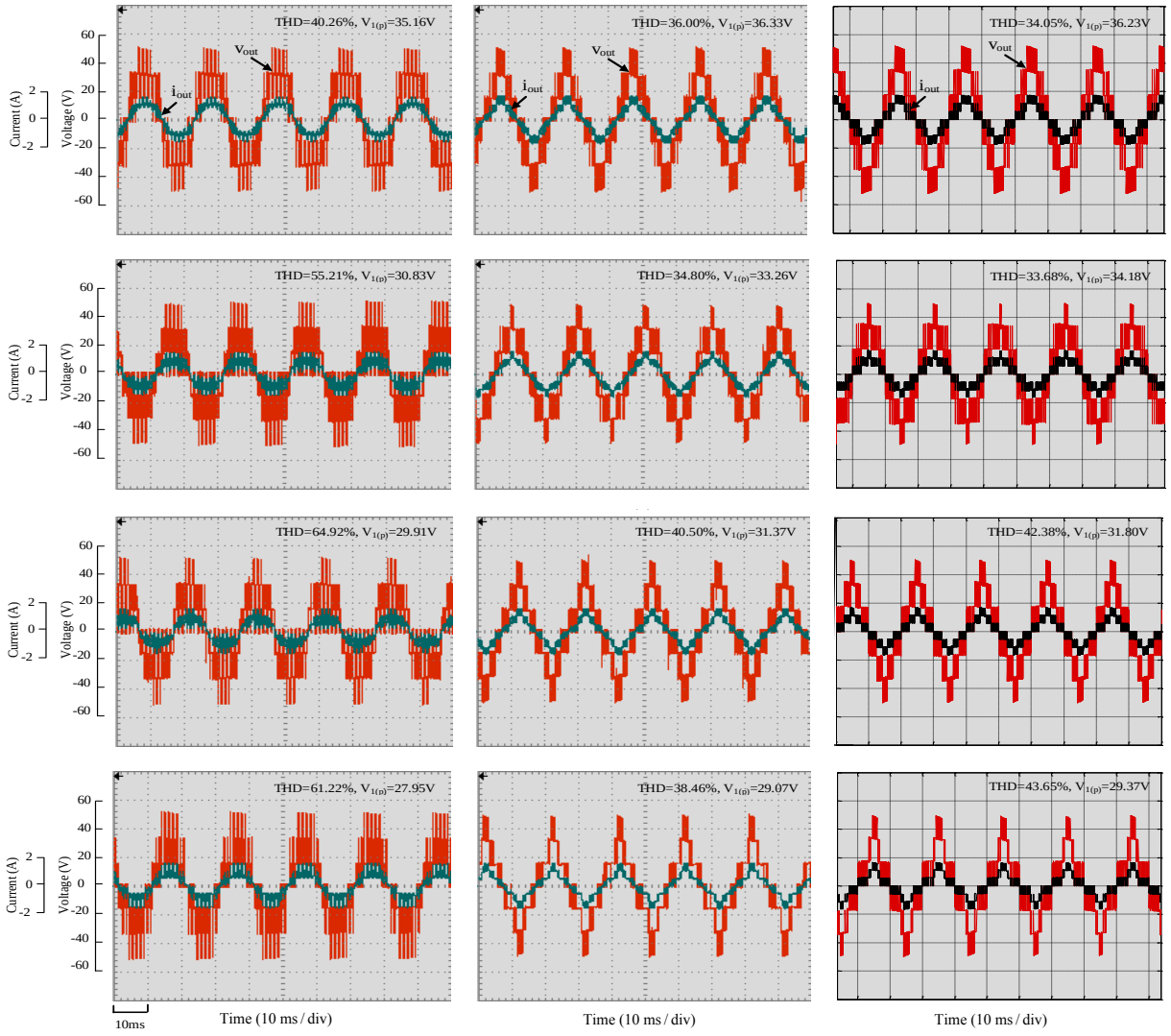

Fig.10: Output voltage and current waveforms of 7-level converter: measured under control by precursor algorithm (column 1); measured and simulated under control by improved algorithm (columns 2 and 3). Irradiances applied to sources PV1, PV2 and PV3 in W/m^2, top to bottom row: (1000, 500, 1000); (1000, 1000, 150); (1000, 750, 250); (500, 1000, 250).

Table 5 lists the numerical values obtained by measurements and simulation of the power delivered to the load when the improved control algorithm is applied. The small discrepancies between measured and simulated results are principally caused by the inverter losses which were not accounted for in simulations.

Extracted power (W)			Precursor algorithm Measured results		Improved algorithm Measured results		Improved algorithm Simulated Results	
PV1	PV2	PV3	THD (%)	$V_{1(P)}$ (V)	THD (%)	$V_{1(P)}$ (V)	THD (%)	$V_{1(P)}$ (V)
10	5	10	40.26	35.16	36.00	36.33	34.05	36.23
10	10	1.5	55.21	30.83	34.80	33.26	33.68	34.18
10	7.5	2.5	64.92	29.91	40.50	31.37	42.38	31.80
5	10	2.5	61.22	27.95	38.46	29.07	43.65	29.37

Table 4: Summary of measured and simulated results at various shading levels

Extracted power (W)			Measured Load Power (W)	Simulated Load Power (W)
PV1	PV2	PV3		
10	10	10	28.89	29.96
10	5	10	23.81	24.96
10	10	1.5	21.01	21.44
10	7.5	2.5	19.34	19.98
5	10	2.5	17.20	17.49

Table 5: Measured and simulated values of power delivered to the load at various shading levels

6 Conclusions

The main features of the newly developed control scheme, which uses the VH P&O method and improved PV source PWM permutation algorithm, are: (i) the upholding of operation of all PV sources (shaded or not shaded) at their MPPs, (ii) the delivery of all extracted power from PV sources to the load and (iii) the generation of improved multilevel voltage waveforms with low THD.

The proposed system was simulated using Matlab–Simulink for multilevel DC link converters with five, seven, nine and eleven-level AC output voltages. Static and dynamic irradiance levels were applied to test the system behaviour with respect to the MPP tracking and the quality of the output waveforms. The comparison between the previous and the improved algorithm have shown that the latter generates a lower distortion of the waveform and higher amplitude of the fundamental (50-Hz) harmonic of the output voltage. Experimental tests on a small-scale system, which uses three PV sources and seven-level DC-link converter, have validated the advantages of the new scheme.

The time varying irradiance levels were applied to test dynamic behaviour of the system in terms of the MPP tracking. The algorithm enables the recovery of each shaded PV source to its MPP without affecting other PV sources connected in the chain.

Appendix

When C = 1:

If $v_{offset1}$ is either 0 or 1 and $v_{offset2} = 0$, then:

SW1 is ‘on’ during interval t_{on1} and ‘off’ otherwise;

SW2 is ‘off’ during entire period T_s.

If $v_{offset1} = 0$ and $v_{offset2} = 1$, then:

SW1 is ‘off’ and SW2 is ‘on’ during entire period T_s.

If $v_{offset1} = 1$ and $v_{offset2} = 1$, then:

SW1 is ‘on’ during interval t_{on1} and ‘off’ otherwise;

SW2 is ‘on’ during entire period T_s.

When C = 2:

If $v_{offset2}$ is either 0 or 1 and $v_{offset1} = 0$, then:

SW1 is ‘off’ during entire period T_s;

SW2 is ‘on’ during interval t_{on2} and ‘off’ otherwise.

If $v_{offset2}$ is 0 and $v_{offset1} = 1$, then:

SW2 is ‘off’ and SW1 is ‘on’ during entire period T_s.

If $v_{offset1} = 1$ and $v_{offset2} = 1$, then:

SW1 is ‘on’ during entire period T_s;

SW2 is ‘on’ during interval t_{on2} and ‘off’ otherwise.

In Fig. A1, v_{ref1} and v_{ref2} are two reference voltages of the five-level converter. These signals are sampled at periods T_s yielding M_f samples for each reference signal over the time period $T_r = 1/f_r$. (f_r denotes the required output frequency, e.g. 50 Hz.) At each period T_s, the sampled values are applied to the Eqs. (1) - (3) for generating the required control signals.

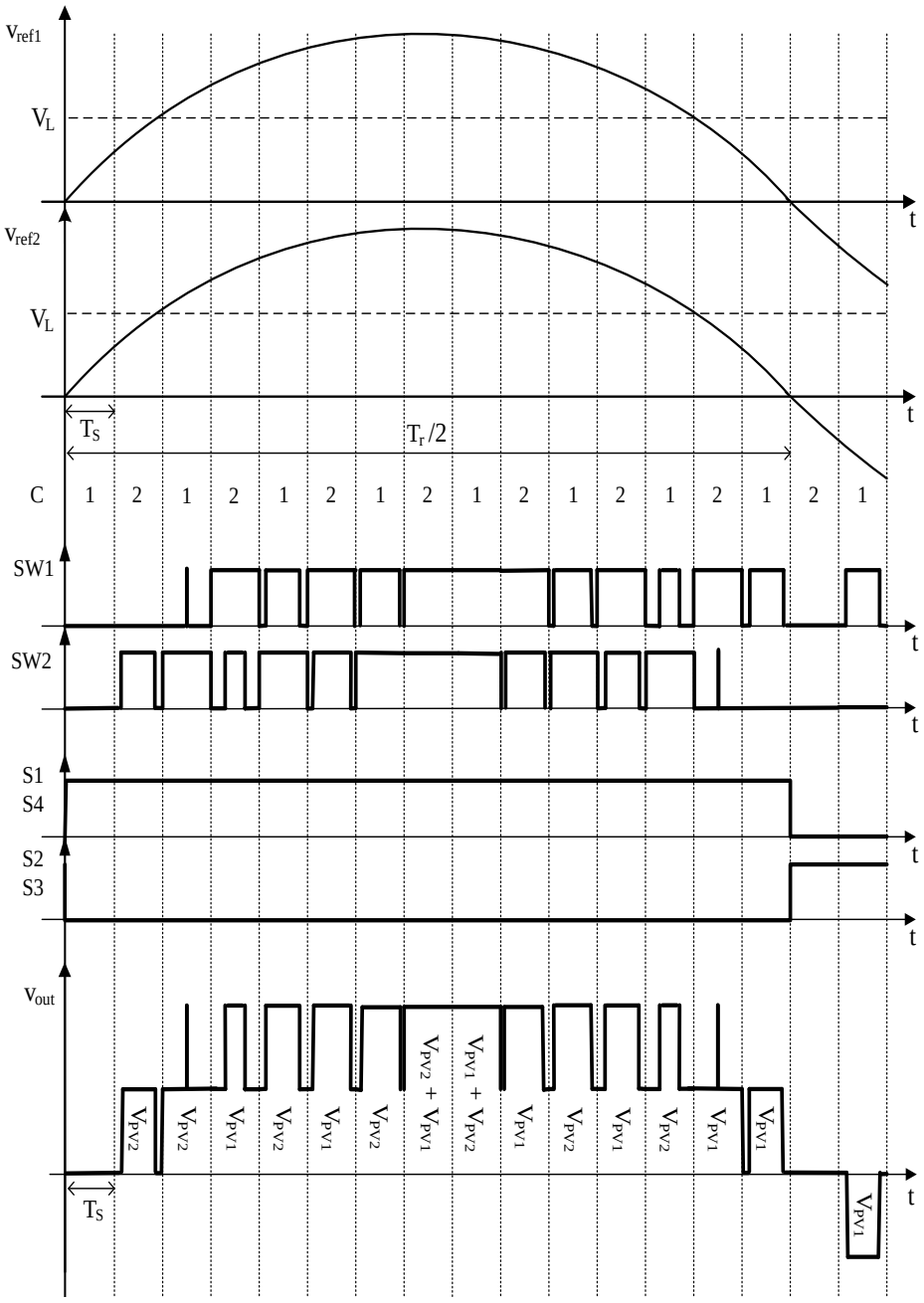

Fig. A1: Graphical illustration of the process for generating the output waveform in the basic system with two PV sources

References

[1] G. R. Walker, P. C. Sernia, "Cascaded DC-DC converter connection of photovoltaic modules", IEEE Trans. Power Electronics, vol.19, no.4, pp.1130-1139, July 2004.

[2] E. Roman, R. Alonso, P. Ibanez, S. Elorduizapatarietxe, D. Goitia, "Intelligent PV Module for Grid-Connected PV Systems", IEEE Trans. Industrial Electronics, vol.53, no.4, pp.1066-1073, June 2006.

[3] B. Chong, L. Zhang, "Controller Design for Integrated PV-Converter Modules under Partial Shading Conditions", ELSEVIER Journal of International Solar Energy Society, vol.92, pp.123-138, 2013.

[4] S. Busquets-Monge, J. Rocabert, P. Rodriguez, S. Alepuz, J. Bordonau, "Multilevel Diode-Clamped Converter for Photovoltaic Generators With Independent Voltage Control of Each Solar Array", IEEE Trans. Industrial Electronics, vol.55, no.7, pp.2713-2723, July 2008.

[5] L. Gao, R. A. Dougal, S. Liu, A. Iotova, "Parallel-connected solar PV system to address partial and rapidly fluctuating shadow conditions", IEEE Trans. Ind. Electron., vol. 56, no. 5, pp. 1548–1556, May 2009.

[6] G. Velasco, J. J. Negroni, F. Guinjoan, R. Pique, "Energy generation in PV grid-connected systems: power extraction optimization for plant oriented PV generators", IEEE International Symposium on Industrial Electronics (ISIE), vol.3, pp.1025-1030, 2005.

[7] G. Velasco-Quesada, F. Guinjoan-Gispert, R. Pique-Lopez, M. Roman-Lumbreras, A. Conesa-Roca, "Electrical PV Array Reconfiguration Strategy for Energy Extraction Improvement in Grid-Connected PV Systems", IEEE Trans. Industrial Electronics, vol.56, no.11, pp.4319-4331, Nov. 2009.

[8] T. Shimizu, M. Hirakata, T. Kamezawa, H. Watanabe, "Generation control circuit for photovoltaic modules", IEEE Trans. Power Electronics, vol.16, no.3, pp.293-300, May 2001.

[9] Qi Zhang, Xiangdong Sun, Yanru Zhong, Mikihiko Matsui, "A novel topology for solving the partial shading problem in photovoltaic power generation system", IEEE 6th International Power Electronics and Motion Control Conf. (IPEMC '09), pp.2130-2135, 2009.

[10] S. J. Lee, H. S. Bae, B. H. Cho, "Modeling and control of the single-phase photovoltaic grid-connected cascaded H-bridge multilevel inverter", IEEE Energy Conversion Congress and Exposition Conf. (ECCE'09), pp.43-47, 2009.

[11] I. Abdalla, J. Corda, L. Zhang, "Multilevel DC-Link Inverter and Control Algorithm to Overcome the PV Partial Shading," IEEE Trans. Power Electronics, vol.28, no.1, pp.14-18, Jan. 2013.

[12] D. Ning-Yi, W. Man-Chung, C. Yuan-Hua, H. Ying-Duo, "A 3-D generalized direct PWM algorithm for multilevel converters", IEEE Letters. Power Electronics, vol.3, no.3, pp.85-88, 2005.

[13] J. H. R. Enslin, "Maximum Power Point Tracking: A Cost Saving Necessity in Solar Energy Systems", 16th Annual Conference of IEEE Industrial Electronics Society (IECON '90), pp. 1073-1077, 1990.

[14] K. H. Hussein, I. Muta, T. Hshino, and M. Osakada, “Maximum photovoltaic power tracking: an algorithm for rapidly changing atmospheric conditions,” IEE Procceedings – Generation, Transmission and Distribution, vol. 142, no.1, pp. 59-64, 1995.

[15] C. Hua, J Lin and C. Shen, "Implementation of a DSP-Controlled Photovoltaic System with Peak Power Tracking", IEEE Transactions on Industrial Electronics, vol.45, no.1, pp. 99-107, 1998.

[16] M. Matsui, T. Kitano, D. Xu and Z. Yang "A New Maximum Photovoltaic Power Tracking Control Scheme based on Power Equilibrium at DC Link", Conference Record of the IEEE Thirty-Fourth IAS Annual Meeting, vol.2, pp. 804-809, 1999.

[17] N. Kasa, T. Iida and H. Iwamoto, "Maximum Power Point Tracking with Capacitor Identificator for Photovoltaic Power System", Eighth International Conference on Power Electronics and Variable Speed Drives, IEE Conf. Publ. No.475, pp. 130-135, 2000.

[18] E. Koutroulis, K. Kalaitzakis and N. C. Voulgaris, "Development of a Microcontroller-based Photovoltaic Maximum Power Point Tracking Control System", IEEE Trans. on Power Electronics, vol.16, no.1, pp.46-54, 2001.

[19] M. Veerachary, T. Senjyu, and K. Uezato, "Voltage-based maximum power point tracking control of PV system", IEEE Trans. Aerosp. Electron. Syst., vol.38, no.1, pp.262-270, 2002.

[20] R. D. Middlebrook and S. Cuk, "A generalized unified approach to modelling switching-converter power stages", IEEE Power Electronics Specialist Conference, PESC'76 Record, pp.18-34, 1976.

[21] I. Abdalla, “Integrated PV and multilevel converter system for maximum power generation under partial shading conditions”, PhD Thesis, University of Leeds, UK, 2013.

[22] Texas instruments, TMS320F28335 Data Manual, 2010.